

The Role of Ceramics in Transforming Industries

Applications and Future Developments

EBOOK 18



Contents

- 3 Introduction
Ceramics: Unveiling the Versatility and Challenges of a Revolutionary Material

- 5 Local and High-Strength Joining of Transparent Glass and Glass-Ceramics by Femtosecond Bessel Beam
Adapted from Fedotov, S. et al., 2023

- 8 Multi-Objective Optimization During Magnetic Field Assisted ECDM of Alumina-Zirconium Dioxide Ceramic Composite Using Battle Royale Optimization
Adapted from Soni, D. et al., 2023

- 11 Engineering Dislocation-Rich Plastic Zones in Ceramics via Room-Temperature Scratching
Adapted from Fang, X. et al., 2023

- 14 About the Sponsor: Seeing is Solving

Imprint

© Wiley-VCH GmbH
Boschstr. 12,
69469 Weinheim, Germany
Email: info@wiley-vch.de
Editors: Dr. Cecilia Kruszynski &
Róisín Murtagh

Ceramics: Unveiling the Versatility and Challenges of a Revolutionary Material

Ceramics comprehend a fundamental class of materials that plays a crucial role in various applications. In the context of materials science, ceramics refer to a broad category of inorganic, non-metallic solids primarily composed of compounds between metallic and non-metallic elements. These materials are typically crystalline in nature and are known for their excellent mechanical, thermal, electrical, and chemical properties. Ceramics encompass a wide range of compositions, including oxides, carbides, nitrides, and more, each exhibiting distinct properties and behavior.

Among their many attributes, ceramics are particularly distinguished by their exceptional hardness, high melting points, and low electrical and thermal conductivity. They often possess excellent wear and corrosion resistance and can endure extreme conditions. On the other hand, a common drawback of ceramic materials is their inherent brittleness, which has to be taken into account in the design of ceramic pieces, to mitigate potential issues.

Ceramics find significant application across diverse industries, including aerospace, automotive, electronics, healthcare, energy, and more. They are widely utilized for manufacturing cutting-edge components such as insulators, sensors, cutting tools, bio-ceramic implants, electronic substrates, and thermal barriers, to name a few [1–4]. Their use in these industries is driven by their unique properties that contribute to enhanced performance and efficiency.

In many cases, these materials are chosen over traditional materials like metals and polymers due to their superior properties. They are particularly favored in high-temperature environments, aggressive chemical settings, and applications demanding high wear resistance. Ceramics are indispensable in scenarios where other materials would not withstand the extreme conditions or provide the necessary performance levels.

Ceramic components are typically shaped into desired forms from a blend of powder, sometimes with binders and other enhancements, using established methodologies like injection molding, die pressing, tape casting, and gel casting, among others [5]. Achieving densification necessitates sintering the green parts at elevated temperatures. However, these traditional ceramic forming techniques pose limitations due to prolonged processing durations and elevated costs. Moreover, they struggle to create intricate structures with complex geometries and interconnected voids, primarily because molding is a crucial step in these approaches.

Conversely, the machining of ceramic components is exceptionally challenging due to their inherent brittleness and exceptional hardness. Techniques such as grinding, polishing, laser cutting, and electrical discharge machining are employed to achieve precise shapes and surface finishes. The hardness of ceramics poses difficulties during machining, causing substantial wear on cutting tools. Additionally, the machining process can introduce defects such as cracking in the ceramic parts, further complicating efforts to attain precise dimensional accuracy and a smooth surface finish. These inherent challenges in ceramic machining contribute

to the perception that ceramic production involves specialized and cost-intensive processes compared to alternative materials. Despite the initial higher costs, the enduring advantages, durability, and superior performance of ceramics often outweigh the expense, particularly in critical applications where their unique properties are indispensable.

In this context, advanced machining methods are essential to harness the full potential of ceramics in various applications. One example is additive manufacturing techniques, whose implementation would allow the rentable fabrication of high-performance ceramic components at industrial scale [6]. Another advanced method that can significantly improve the productivity and efficiency of ceramic piece production is electrochemical discharge machining (ECDM) [7], a hybrid non-conventional machining technique specifically designed for machining both electrically conductive and non-conductive materials. This method is highly favored for constructing minuscule features, such as micro holes, micro channels, microgrooves, and intricate three-dimensional shapes in ceramic materials.

The pursuit of harnessing the versatile mechanical and functional properties of ceramic materials has driven a surge in research efforts within this burgeoning field. Notably, the deliberate engineering of dislocations stands out as a crucial avenue for tailoring mechanical properties in ceramics [8]. By strategically manipulating dislocations, engineers can precisely design and enhance the mechanical attributes of ceramics, further amplifying their potential in various applications. Dislocations refer to deviations from the perfect crystalline structure within these inorganic, non-metallic materials. These deviations can be linear defects

like edge or screw dislocations. In ceramics, dislocations play a vital role in influencing mechanical properties and behavior, influencing properties, such as fracture toughness, plasticity, and deformation mechanisms. Given the typically brittle nature of ceramics, understanding and controlling dislocations are crucial for enhancing their performance and enabling applications in diverse industries. Engineers and materials scientists study these dislocations to design ceramic materials with improved properties and develop strategies to minimize or control dislocation-related effects, ultimately advancing the potential applications of ceramics in various technological domains.

In the broad scope of characterizing ceramics, a precise knowledge of composition and understanding their fundamental properties and behaviors is pivotal. This understanding facilitates the assessment and optimization of ceramics for varied applications. Within this domain, optical metrology emerges as a critical facet. Optical metrology entails the utilization of specialized optical instruments and techniques to meticulously measure, analyze, and characterize ceramics' bulk and surface. These methods provide essential insights into crucial aspects, such as structural integrity, surface quality, dimensional accuracy, and the overall performance of ceramic components. By ensuring that ceramics adhere to stringent quality standards, optical metrology maximizes their potential and facilitates their optimal utilization across diverse industrial and engineering applications.

Ceramics represent a fascinating class of materials that have revolutionized multiple industries. Their exceptional characteristics and diverse applications make them a subject of significant interest and study.

References:

- [1] Karadimas, G. and Salonitis, K. (2023). *Ceramic Matrix Composites for Aero Engine Applications—A Review*. *Applied Sciences*. DOI: [10.3390/app13053017](https://doi.org/10.3390/app13053017).
- [2] Sahoo, P. et al. (2023). *Smart ceramic coatings used in the automotive industry*, in *Advanced Ceramic Coatings*, Elsevier, pp. 219–231.
- [3] Santhosh, G. (2023). *Anticorrosion and antiwear ceramic coatings*, in *Advanced Ceramic Coatings*, Elsevier, pp. 89–105.
- [4] Randhawa, K. S. (2023). *A state-of-the-art review on advanced ceramic materials: fabrication, characteristics, applications, and wettability*. *Pigment & Resin Technology*. DOI: [10.1108/PRT-12-2022-0144](https://doi.org/10.1108/PRT-12-2022-0144).
- [5] Bengisu, M. (2001). *Engineering Ceramics*, Springer Berlin Heidelberg, Berlin, Heidelberg.
- [6] Dadkhah, M. et al. (2023). *Additive manufacturing of ceramics: Advances, challenges, and outlook*. *Journal of the European Ceramic Society*. DOI: [10.1016/j.jeurceramsoc.2023.07.033](https://doi.org/10.1016/j.jeurceramsoc.2023.07.033).
- [7] Sharma, P. et al. (2020). *Experimental investigations into alumina ceramic micromachining by electrochemical discharge machining process*. *Procedia Manufacturing*. DOI: [10.1016/j.promfg.2020.05.044](https://doi.org/10.1016/j.promfg.2020.05.044).
- [8] Soni, D. et al. (2023). *Multi-Objective Optimization During Magnetic Field Assisted ECDM of Alumina-Zirconium Dioxide Ceramic Composite using battle royale optimization*. *Advanced Engineering Materials*. DOI: [10.1002/adem.202201928](https://doi.org/10.1002/adem.202201928).

01 Local and High-Strength Joining of Transparent Glass and Glass-Ceramics by Femtosecond Bessel Beam

Adapted from Fedotov, S. *et al.*, 2023

This study explores Bessel beam laser welding of phosphate glass and spinel-based glass-ceramic, investigating the dependencies of weld geometry on pulse energy and scanning speed. Optimized laser exposure conditions were identified to enhance welding durability.

INTRODUCTION

Transparent glasses and glass-ceramics find broad applications due to their unique optical properties, chemical durability, and thermal stability. Creating strong joints between materials with differing properties is crucial for microfluidic devices, microchip lasers, and sensors. Femtosecond laser pulses have shown promise in welding technology, potentially surpassing the limitations of other methods like diffusion welding, anodic bonding, CO₂, and solid-state laser welding [1–3].

Typically, Gaussian intensity profile laser beams with high numerical aperture focusing optics were conventionally employed. However, these beams have a small Rayleigh length, requiring precise surface positioning relative to the laser beam waist. Overcoming this limitation involves using a low numerical aperture microscope objective or a laser beam with a Bessel intensity distribution.

This study delves into femtosecond laser welding of phosphate laser glass with magnesium aluminosilicate glass-ceramic, based on nanocrystals of co-doped spinel and magnesium aluminotitanate solid solutions, exhibiting substantially different coefficients of thermal

expansions (CTEs) (110×10^{-7} and $50 \times 10^{-7} \text{ K}^{-1}$, respectively), utilizing a Bessel beam.

MATERIALS

For femtosecond laser welding experiments, we utilized patented phosphate glass with the composition: $51\text{P}_2\text{O}_5 \cdot 24\text{SiO}_2 \cdot 7\text{B}_2\text{O}_3 \cdot 10\text{Al}_2\text{O}_3 \cdot 10\text{BaO} \cdot 17\text{K}_2\text{O} \cdot 1\text{Nd}_2\text{O}_3$ and magnesium aluminosilicate glass-ceramic (MAS:Co) with the composition: $18\text{MgO} \cdot 18\text{Al}_2\text{O}_3 \cdot 55\text{SiO}_2 \cdot 9\text{TiO}_2$ (0.05 wt% CoO added). Prior to laser exposure, samples were polished using diamond grinding disks with various abrasive particle sizes and then finely polished with a disk covered in faux suede and CeO₂ as a polishing agent. Subsequently, samples were tightly clamped using a specialized mandrel.

A laser emitted 180 fs pulses at 1,030 nm wavelength with a 5 kHz pulse repetition rate, providing sufficient pulse energy for welds using a Bessel beam. Laser scanning adopted a transverse scheme, perpendicular to both the sample plane and the sample's translation direction. Pulse energy varied from 0.5 to 8 μJ , and scanning speed varied from 0.2 to 2.1 mm/s.

To maintain uniform polarization effects, a quarter-wave plate was introduced into the optical path. The Bessel intensity distribution was achieved using a silica glass axicon with a 2° base angle. The optical setup included a 4f-system comprising a lens with $f = 250$ mm and an objective with $f = 18$ mm (Olympus LMPlan N 10x, NA = 0.3). This configuration reduced the Bessel beam size, reproduced it on the materials' interface, and ensured high peak intensity at the focal region.

The focal depth after the 4f-system was approximately 1.3 mm, with the core diameter of the Bessel beam at about $4.6 \mu\text{m}$ after demagnification. Laser light was focused onto the materials interface through phosphate glass, and the resulting tracks were examined using a brightfield optical microscope (Olympus BX51).

RESULTS

We examined laser-written track geometry (height, width) dependence on laser exposure conditions, presented in Figure 1a,b as brightfield optical images at the glass–glass–ceramic interface. Precisely delineating track boundaries is challenging due to blurred edges along the laser propagation. Therefore, we quantitatively estimated weld height by measuring the increase in transmitted light intensity to the $1/e$ level.

Figure 1b,c illustrates the relationship between track height and width at the material interface concerning pulse energy and scanning speed. Scanning speed (0.4–2 mm/s) minimally affects track height, maintaining it around $750 \mu\text{m}$ (Fig. 1c). Weld width primarily responds to pulse energy, with a minimum of about $2.2 \mu\text{J}$ needed for effective laser welding. Pulse energy increased to about $4.5 \mu\text{J}$ (Fig. 1d) widens the weld from 2 to $3.5 \mu\text{m}$ approximately, plateauing at higher pulse energies.

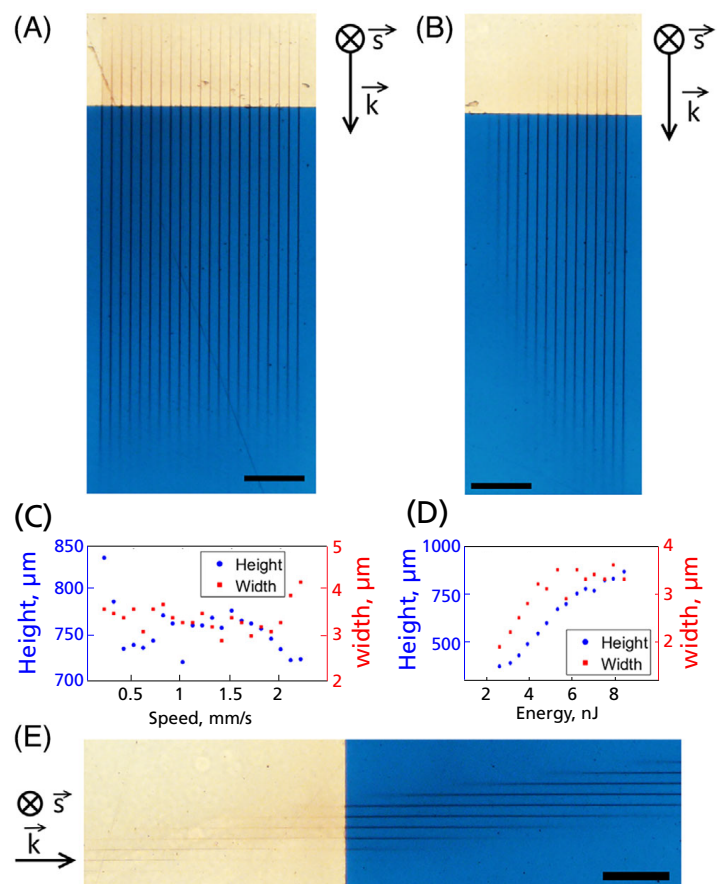


Figure 1. (a and b) Brightfield optical images of a face view of the series of welds formed at various scanning speeds and pulse energy, respectively; (c) Dependence of the weld height and width on scanning speed ($E = 6.5 \mu\text{J}$); (d) Dependence of the track height and width on pulse energy ($V = 1$ mm/s); (e) Brightfield optical images of welds face view, written at different positions of Bessel beam relatively to materials interface. The scale bar is $120 \mu\text{m}$.

Track height is highly adjustable, ranging from 450 to 800 μm , by varying pulse energy. It grows rapidly up to 6–6.5 μJ , slowing at higher pulse energies. Utilizing the Bessel beam for laser welding enables substantial vertical focus position variation, from +250 to –250 μm , with 0 μm signifying the material interface and Bessel beam-written track center (Fig. 1e).

Notably, when welding closely adjacent materials, the range of focus variation narrows due to laser-induced stress accumulation. Accumulated stress causes crack generation in phosphate glass, resulting in joint failure upon mandrel release. Given glass-ceramics' superior strength and crack resistance compared to phosphate glass, adjusting the focus position deeper within the Glass-ceramic sample proved advantageous.

Laser welding utilized 6.5 μJ pulse energy and 1 mm/s scanning speed, resulting in a 1.98 mm² joint area with 100 concentric welds (7 μm step). Laser-written welds cover about 35% of the joint area, and negligible contribution of the area between seams to shear strength was confirmed [4].

In Figure 2a, optical contact forms a ring-shaped joint between glass and glass-ceramics, with visible interference fringes indicating increasing gap distance. Optical microscopy (Fig. 2b) revealed scratches and gouges due to high microhardness from the spinel crystalline phase. Glass-ceramic surface roughness (260 \pm 15 nm) confirms Bessel beam tolerance. However, laser beam scattering through surface

defects causes weld seam inhomogeneities. High surface roughness hampers strong optical contact, justifying area neglect between seams in joint area calculation.

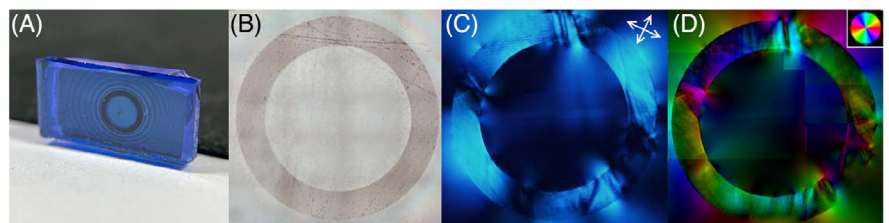
Cross-polarized (Fig. 2c) and pseudocolor images (Fig. 2d) display laser-induced mechanical stress, showing substantial, uneven distribution likely due to inadequate polishing, scratches, or gouges.

Strength testing revealed shear strength ranging from 64 to 147 MPa across four samples (average: 96 \pm 40 MPa). Variability arises from sample count, surface quality, and stress distribution. Two joints had small cracks, resulting in lower shear strength (64–67 MPa). Importantly, even the minimal strength surpasses previous maximums for laser-welded glass and glass-ceramics, considering their closed CTE [5].

CONCLUSIONS

In summary, femtosecond laser welding of glass and glass-ceramic plates using a Bessel intensity distribution beam was showcased. Weld seam width primarily correlates with pulse energy, with scanning speed showing lesser impact within the studied laser exposure ranges. Shear strength testing revealed impressive values, reaching up to 147 MPa, displaying potential for high-power microchip lasers with passive Q-switching using these materials. These results underline femtosecond lasers' efficiency in industrial welding across diverse materials.

Figure 2. (a) Photograph of welded samples; stitched optical images of the weld: (b) In brightfield mode, (c) In crossed polarizers (arrows indicate the orientation of polarizer and analyzer); (d) Pseudocolor image of the distribution of the slow axis of birefringence (brightness shows optical retardance).



References:

- [1] Fedotov, S. et al. (2023). Local and high-strength joining of transparent glass and glass-ceramics by femtosecond Bessel beam. *Journal of the American Ceramic Society*. DOI: 10.1111/jace.19391.
- [2] MacCallum, D.O. et al. (2005). CO₂ laser welding fused silica. *International Congress on Applications of Lasers & Electro-Optics*. DOI: 10.2351/1.5060423.
- [3] Younger, P.R. (1980). Hermetic glass sealing by electrostatic bonding. *Journal of Non-Crystalline Solids*. DOI: 10.1016/0022-3093(80)90553-0.
- [4] Hélié, D. et al. (2012). Reinforced direct bonding of optical materials by femtosecond laser welding. *Applied Optics*. DOI: 10.1364/AO.51.002098.
- [5] Richter, S. et al. (2016). Laser welding of glasses at high repetition rates – Fundamentals and prospects. *Optics & Laser Technology*. DOI: 10.1016/j.optlastec.2016.03.022.

02 Multi-Objective Optimization During Magnetic Field Assisted ECDM of Alumina-Zirconium Dioxide Ceramic Composite Using Battle Royale Optimization

Adapted from Soni, D. et al. 2023

Alumina-zirconium dioxide ($\text{Al}_2\text{O}_3\text{-ZrO}_2$) ceramic composite material (CCM) is prized for superior mechanical and corrosion resistance, and is widely used in industrial components. Here, electrochemical discharge machining is explored for efficient CCM machining, leveraging a magnetic field to boost the material removal rate.

INTRODUCTION

Ceramic and ceramic matrix composites pose machining challenges due to brittleness, abrasiveness, and high hardness. Traditional methods are ineffective for these materials, prompting exploration of nontraditional approaches like electrochemical discharge machining (ECDM). ECDM, combining electrical discharge machining (EDM) and electrochemical machining (ECM) features, proves effective for machining hard materials. It employs discharge phenomena and thermal effects, facilitating material removal, especially in micro-hole drilling for ceramic composites utilized in aerospace, electronics, and automobiles. $\text{Al}_2\text{O}_3\text{-ZrO}_2$, widely used in gas turbines and heat exchangers, is micro-drilled using ECDM in this study. Adding alumina and cerium oxide nanoparticles to the dielectric medium enhances machinability by reducing surface roughness and increasing material removal rate (MRR). The nanoparticles modify electrolyte thermal conductivity, inducing more thermal energy and improving machinability. The research focuses on machining time (MT) and taper angle (TA) in ECDM of $\text{Al}_2\text{O}_3\text{-ZrO}_2$, employing battle royale optimization (BRO) as

a metaheuristic algorithm to optimize ECDM parameters, validated using a modified deep belief network (DBN).

EXPERIMENTAL SECTION

This study drilled 3 mm thick $\text{Al}_2\text{O}_3\text{-ZrO}_2$ of size 20 mm × 20 mm, using a computer numerical control (CNC) electrochemical discharge machine. The electrolyte used is NaOH; 50 ppm of alumina and cerium oxide nanoparticles of size ca. 20 nm are also added to the electrolyte to enhance its thermal and electrical conductivity effectively [1]. Initially, a preliminary analysis was conducted to select the input parameters. To optimize the ECDM process, a modern meta-heuristic algorithm called battle royale optimization (BRO) is used [2].

The experiments were conducted using a homemade ECDM machine with a workbench size of 450 × 450 mm. A 20 × 5 × 3.5 mm (outer diameter × inner diameter × thickness) Nd-Fe-b ring magnet (0.26 ± 0.01 T) was added to the tool spindle collection to provide a magnetic field during the process [3]. The ECDM machine has an acrylic chamber where the workpiece and electrolytes are placed.

A CNC software-aided control unit controlled the workbench XYZ movements.

During experimentation, the 2 mm diameter tungsten carbide tool electrode (cathode) was mounted on the tool chuck. The acrylic tank was filled with specifically prepared nanoparticle-added NaOH electrolytes up to a particular level (2 mm above the top surface of the workpiece). The negative terminal of the DC power supply unit was connected to the tool through a carbon brush to maintain the tool electrode as the cathode. In contrast, the positive terminal was connected to a graphite auxiliary electrode inserted into the electrolyte. The experiments were conducted by setting up several constant input parameters [4]. The pulse on time, pulse off time, supplied current, and duty cycle were constant parameters (40 pulses on time, 25 pulses off time, 15 A current, and 70% duty cycle).

RESULTS AND DISCUSSION

The experiment was conducted three times at all input conditions. Several ECDM response parameters like MRR, entrance overcut (EO), TA, and MT were calculated for each experiment. TA and EO were obtained by examining the surface of a machined workpiece using an Olympus DSX100 3D digital microscope [5]. Simultaneously, the MRR was determined by comparing the weights of a workpiece before and after drilling each hole, as shown in Equation 1 [6]. The average of the MRR, EO, TA, and MT measurements was calculated for each set of observations and considered for further study.

$$MRR = \frac{W_b - W_a}{t} \quad (\text{mg min}^{-1})$$

Equation 1. Where W_b and W_a are the weights of the workpiece before and after machining, and t represents the total machining time.

As depicted in Figure 1, the MRR demonstrates an upward trend as both voltage and electrolyte concentration increase. In Figures 1a and 1b, with the inter-electrode gap set at 40 and 50 mm, it becomes evident that a 50 mm inter-electrode gap (IEG) results in a lower MRR for lower electrolyte concentration (EC) and applied voltage (AV). It indicates that poor gas bubble formation at lower values of voltage and EC has no significant effect on MRR for any

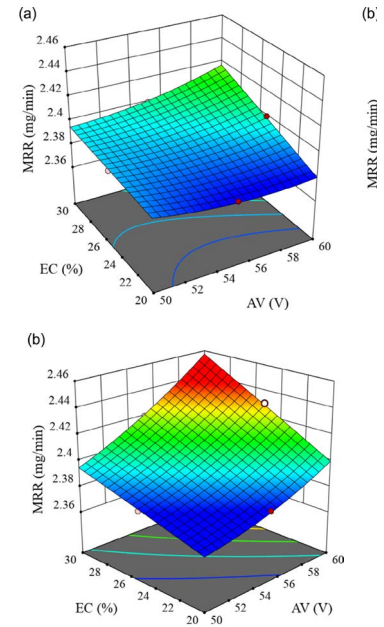


Figure 1. Influence of ECDM parameters on MRR. a) At IEG = 40 mm; b) At IEG = 50 mm.

level of IEG. Moreover, higher spark intensity and discharge energy at 30% of EC and 60 V of AV evaporated more material from the workpiece surface than their lower levels. Relatively, less side sparking at smaller IEG could be another reason for such a lower MRR at lower values of IEG. The maximum MRR obtained during the experiment was 2.44 mg min^{-1} at 2nd experiment run. In contrast, the minimum MRR is recorded at run 9 as 2.38 mg min^{-1} .

According to the results, the EO was slightly higher for higher values of EC and IEG. This indicates that although more bubble formation occurs at a higher voltage supply, the magnetic field helped spread gas bubbles across the entire surface rather than just concentrating at the entrance of the cut. However, as EC and AV, have very less influence on the EO during observation.

The TA throughout the machined hole was noticed as a minimum for all samples at fewer values of EC and AV. The lower TA was mainly due to the lower viscosity of electrolyte at minimum EC and reduced electrolyte discharge at minimum AV. Also, an increase in IEG significantly lowered the flow of ions between the anode and cathode. Therefore, the reduction in gas film formation and spark generation thus helped to achieve lower TA.

The MT reduces with an increase in MRR. Therefore, the MRR and MT are the mutual responses of the ECDM process. As the MRR get increased with an increase in EC and AV, the time required to complete the hole profile was minimal at this input level.

CONCLUSIONS

The electrochemical discharge machining on $\text{Al}_2\text{O}_3\text{-ZrO}_2$ ceramic composite material was done with the help of a CNC ECDM machine. The study used different input combinations of various AV, EC, and IEG process parameter levels to machine 2 mm hole on 3 mm depth work material. The optimum ECDM conditions for obtaining the best results were 55 V applied voltage, 22.727% electrolytic concentration, and 40.909 mm inter electrode gap, respectively.

The achieved MRR, EO, TA, and MT values from these input conditions are $2.218 \text{ mg min}^{-1}$, $0.083 \mu\text{m}$, 2.655° , and 884.545 s.

The relationship between MRR, EO, TA, and MT ECDM responses and AV, EC, and IEG process parameters on $\text{Al}_2\text{O}_3\text{-ZrO}_2$ ceramic composite material was studied experimentally and numerically. Future parameters, such as duty cycle, electrode spin speed, the direction of electrode rotation, etc., could be studied on such responses. Besides, the microscopic analysis of the machined workpiece and tool electrode will be established in future experiments. Further, this study can be extended by trying different types of hybrid electrolytes and deep neural network based performance evaluations.

References:

- [1] Elhami, S. and Razfar, M.R. (2020). Application of nano electrolyte in the electrochemical discharge machining process. *Precision Engineering*. DOI: [10.1016/j.precisioneng.2020.03.010](https://doi.org/10.1016/j.precisioneng.2020.03.010).
- [2] Rahkar Farshi, T. (2021). Battle royale optimization algorithm. *Neural Computing and Applications*. DOI: [10.1007/s00521-020-05004-4](https://doi.org/10.1007/s00521-020-05004-4).
- [3] Cheng, C.-P. et al. (2010). Magnetic field-assisted electrochemical discharge machining. *Journal of Micromechanics and Microengineering*. DOI: [10.1088/0960-1317/20/7/075019](https://doi.org/10.1088/0960-1317/20/7/075019).
- [4] Zheng, Z.-P. et al. (2007). The tool geometrical shape and pulse-off time of pulse voltage effects in a Pyrex glass electrochemical discharge microdrilling process. *Journal of Micromechanics and Microengineering*. DOI: [10.1088/0960-1317/17/2/012](https://doi.org/10.1088/0960-1317/17/2/012).
- [5] Arab, J. et al. (2021). Effect of tool-electrode material in through-hole formation using ECDM process. *Materials and Manufacturing Processes*. DOI: [10.1080/10426914.2021.1885700](https://doi.org/10.1080/10426914.2021.1885700).
- [6] Goud, M. and Sharma, A.K. (2017). On performance studies during micromachining of quartz glass using electrochemical discharge machining. *Journal of Mechanical Science and Technology*. DOI: [10.1007/s12206-017-0236-8](https://doi.org/10.1007/s12206-017-0236-8).

03 Engineering Dislocation-Rich Plastic Zones in Ceramics via Room-Temperature Scratching

Adapted from Fang, X. et al., 2023

This study proposes a method involving cyclic scratching to induce a plastic zone with increased dislocation density in ceramics at room temperature, providing a potential method for enhancing mechanical and functional properties in various ceramics.

INTRODUCTION

Ceramic and ceramic matrix composites pose recent promising proofs-of-concept for using dislocations in ceramics to harvest versatile mechanical and functional properties have encouraged increasing research endeavors in this rising field. Regardless of the exciting new findings, it remains a great challenge to engineer dislocation structures, particularly at room temperature, into normally brittle ceramics that are prone to cracking.

High-temperature deformation significantly escalates energy consumption and extends the process duration due to the heating process. On the other hand, deformation at room temperature could mitigate energy usage; however, it introduces a greater risk of sample fracturing when experiments are conducted under unfavorable mechanical loading conditions. So far, the majority of works for room-temperature plastic deformation while suppressing crack formation in ceramics were performed at nano-/microscale using nano-indentation tests [1,2] or micropillar compression [3]. However, these nano-/microscale approaches greatly limit the size of the attainable plastic zone.

Here, we propose a simple but powerful approach to cyclically scratch the sample surface in order to achieve a plastic zone up to the micrometer or centimeter range.

EXPERIMENTAL SECTION

Un-doped, single-crystal (001) SrTiO₃ was used for the scratching tests on a universal hardness-testing machine and mounted with a Brinell indenter and a controllable moving single-axis stage. The samples have a minimum thickness of 1 mm, with the side lengths varying from 5 to 10 mm. A hardened stainless-steel spherical indenter with a tip diameter of 2.5 mm was used for the cyclic scratching. During the scratching tests, the indenter was first placed in contact with the sample mounted on the moving stage, which is controlled by a computer program for setting the speed of the stage (0.5 mm/s). For validating the method on other materials, we further tested (001) MgO, (001) ZnS, and (111) CaF₂ surfaces. A load of 1 kg is chosen for all the samples, except for 0.8 kg on ZnS, which was tested in darkness to avoid cracking [4]. Silicone oil was used as a lubricant to reduce wear of the tip as well as crack formation after a high number of scratching cycles.

The dislocation density and etch pit patterns in the plastic zone were characterized with a laser confocal microscope (LEXT™ OLS4000, Olympus) for better identification of surface features (e.g., dislocation etch pits) after surface etching.

RESULTS

The depth changes in the scratch tracks resulting from different numbers of scratches were measured with the confocal laser microscope. In Figure 1, the scratch track depth is approximately 170 nm after a single scratch (1x), increasing to around 300 nm after 10 scratches (10x). Given the scratch track's width of approximately 125 μm , the observed surface undulation across the track can be deemed negligible.

Inside the scratch tracks, we observe numerous horizontal and vertical slip traces, which correspond to intersections of $\{110\}$ slip planes with the (001) surface being scratched. When indenting on the (001) surface of SrTiO_3 , four equivalent slip planes (101), ($\bar{1}01$), (011), and (0 $\bar{1}1$) with a 45° inclination to the indented surface can be activated [5,6]. An increase in the number of slip traces from 1x to 10x is

an indication of an increase in the dislocation density, as will be confirmed later by the chemical etching method [6]. A slight widening of the scratch track is also observed.

The increase of dislocation density as a function of increased scratching cycle number is attributed to dislocation multiplication mechanism, akin to effects in the large spherical ball indentation [5]. The multiplication of the dislocations inside one slip plane is most likely dominated by Frank-Read sources [7], while the formation of a much higher number of slip traces at a higher number of scratching cycles may be governed by cross slip [5], similar to the case of LiF [8]. The major difference here is the stress distribution under ball indentation and ball scratching, which will be investigated in greater detail in future works.

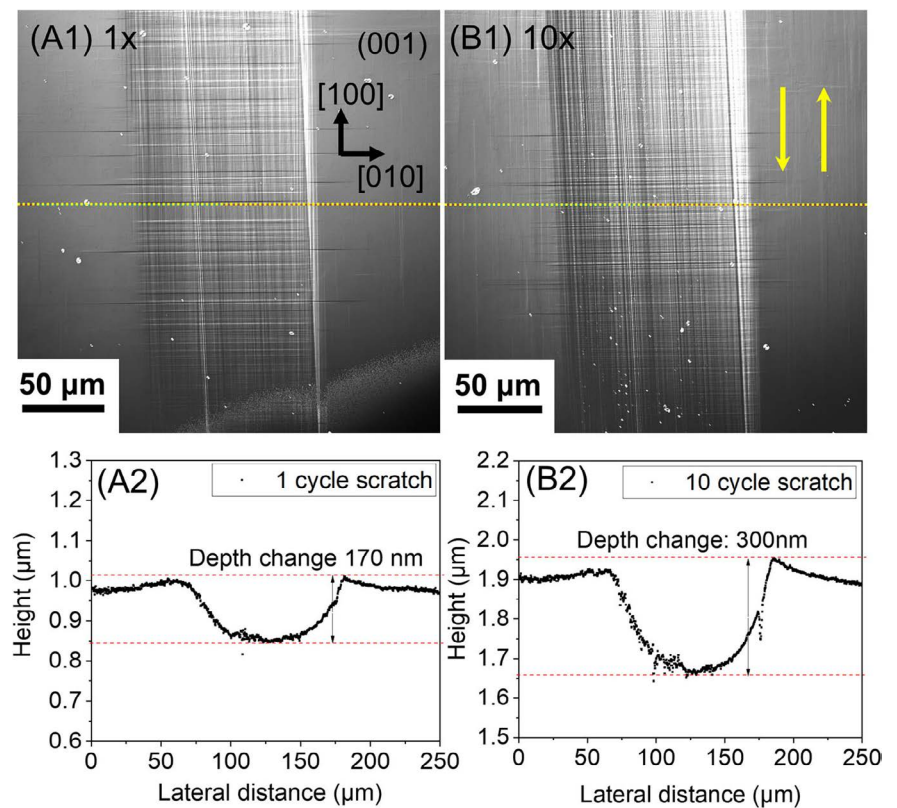


Figure 1. Confocal laser microscope images featuring the surface topography of representative scratch tracks, with the cross-sectional profile extracted: (A1-2) 1x scratch; (B1-2) 10x scratch. The yellow arrows in B1 indicate the (repeated) scratching directions.

CONCLUSION

We demonstrate a simple but powerful experimental method to efficiently increase the dislocation-mediated plastic zone in various ceramics at room temperature. By using a large Brinell indenter (2.5 mm in diameter) for cyclic scratching on the surface of single-crystal SrTiO₃, we succeeded in engineering continuous plastic zones with arbitrary lengths depending on the sample size. After 10 cycles of repetitive scratching inside the same scratch track, a saturation of slip lines, as well as dislocation density inside the plastic zone, was

identified, with the dislocation density above 10¹³ m⁻². This simple technique guarantees sufficiently large plastic volumes with high dislocation density for future assessment of dislocation-tuned functional and mechanical properties. The applicability of this experimental approach is further validated on single crystal MgO, ZnS, and CaF₂, all at room temperature. This experimental approach may hold great potential for various ceramics if it is further extended to high-temperature rolling [9].

Copyright: 10.1111/jace.19140
X. Fang, O. Preuß, P. Breckner, et al.
Journal of the American Ceramic Society
© 2023 The Authors. Journal of the
American Ceramic Society
published by Wiley Periodicals LLC on
behalf of American Ceramic Society.

References

- [1] Fang, X. et al. (2021). Nanoindentation pop-in in oxides at room temperature: Dislocation activation or crack formation? *Journal of the American Ceramic Society*. DOI: [10.1111/jace.17806](https://doi.org/10.1111/jace.17806).
- [2] Nakamura, R. et al. (2023). Nanoindentation responses near single grain boundaries in oxide ceramics. *Journal of the American Ceramic Society*. DOI: [10.1111/jace.18887](https://doi.org/10.1111/jace.18887).
- [3] Korte-Kerzel, S. (2017). Microcompression of brittle and anisotropic crystals: recent advances and current challenges in studying plasticity in hard materials. *MRS Communications*. DOI: [10.1557/mrc.2017.15](https://doi.org/10.1557/mrc.2017.15).
- [4] Oshima, Y. et al. (2018). Extraordinary plasticity of an inorganic semiconductor in darkness. *Science*. DOI: [10.1126/science.aar6035](https://doi.org/10.1126/science.aar6035).
- [5] Okafor, C. et al. (2022). Mechanical tailoring of dislocation densities in SrTiO₃ at room temperature. *Journal of the American Ceramic Society*. DOI: [10.1111/jace.18277](https://doi.org/10.1111/jace.18277).
- [6] Javaid, F. et al. (2017). 3D Dislocation structure evolution in strontium titanate: Spherical indentation experiments and MD simulations. *Journal of the American Ceramic Society*. DOI: [10.1111/jace.14626](https://doi.org/10.1111/jace.14626).
- [7] Hull, D. and Bacon, D.J. (2001). *Introduction to Dislocations*, Elsevier Science.
- [8] Johnston, W.G. and Gilman, J.J. (1960). Dislocation Multiplication in Lithium Fluoride Crystals. *Journal of Applied Physics*. DOI: [10.1063/1.1735655](https://doi.org/10.1063/1.1735655).
- [9] Li, Y. and Tan, C. (2023). Enhancing the mechanical properties of ceramics by high-temperature rolling: A first demonstration using alumina. *Journal of the American Ceramic Society*. DOI: [10.1111/jace.18895](https://doi.org/10.1111/jace.18895).

About the Sponsor: Seeing is Solving

EVIDENT is Empowering Solutions Through Advanced Visualization

Formerly a wholly owned subsidiary of Olympus Corporation, Evident separated from Olympus in 2022 to become a standalone company.

Built on 100 years of innovative technology and a strong foundation of industry leadership, we are committed to developing new technologies and delivering world-class customer service. At Evident, we are guided by the scientific spirit—innovation and exploration are at the heart of what we do. Committed to making people's lives healthier, safer, and more fulfilling, we support our customers with solutions that solve their challenges and advance their work.

Evident's Micro Imaging Solutions division manufactures a comprehensive range of optical-technology-based systems—including microscopes and objectives, slide scanners, and cell culture solutions—for life science applications like research, education, clinical pathology, hematology, and IVF as well as nondestructive industrial applications.

Our Test and Measurement division manufactures precision nondestructive testing instruments ranging from video borescopes to phased array and eddy current flaw detectors and X-ray fluorescence analyzers for a wide variety of applications, including maintenance, manufacturing, and environment and natural resources. These products are widely used for quality control, inspection, and measurement.

Evident is a steadfast partner that balances expertise in advanced technologies with approachability, so customers know they can bring us their questions, and we'll be ready with innovative technologies and groundbreaking solutions that support and empower them. Evident is hard-working and laser-focused on the needs of its customers to create modern solutions that are globally available. No matter where you work or what your challenge is, Evident can help.

[Learn more about who they are.](#)